RSC Advances

ROYAL SOCIETY OF CHEMISTRY

www.rsc.org/advances

Study on reversible hydrogen sorption behaviors of $3LiBH_4$/Graphene and $3LiBH_4$/Graphene-10wt%CeF_3 composites

Yingying Zhu [a], Jianxin Zou,* [a,b]Xiaoqin Zeng [a,b]

[a]National Engineering Research Center of Light Alloys Net Forming & State KeyLaboratory of Metal Matrix Composite, Shanghai Jiao Tong University, Shanghai 200240, China

[b]Shanghai Engineering Research Center of Magnesium Materials, Application & School of Materials Science and Engineering, Shanghai Jiao Tong University, Shanghai 200240, China

Abstract

In the present work, two $LiBH_4$ based hydrogen storage composites, namely, $3LiBH_4$/Graphene and $3LiBH_4$/Graphene-10wt%CeF_3, were prepared through ball milling and their hydrogen sorption behaviors were investigated. It was shown that the dehydrogenation kinetics of $3LiBH_4$/Graphene was improved by doping 10wt% of CeF_3, which was attributed to the formation of CeB_6. The rehydrogenation of the $3LiBH_4$/Graphene composite could be achieved under 440^oC with 3.3 MPa hydrogen pressure and the hydrogen absorption capacity reached 7.40 wt% to $LiBH_4$ after 10 h. Further addition of CeF_3 did not improve the rehydrogenation kinetics but reduced the absorption capacity. SEM observations suggested that $LiBH_4$ was confined in graphene wrapper after rehydrogenation, forming "graphene capsules" that helped the regeneration of $LiBH_4$.

Keywords: hydrogen storage composites; $LiBH_4$; graphene; CeF_3; graphene capsules

1.Introduction

Recent years, new forms of clean energy are extensively considered to replace conventional fossil fuels[1,2] due to the global energy and environmental crises. Among different types of new energy resources, hydrogen energy is regarded as a promising one owing to its cleanness, inexhaustible resources and high power density. The utilization of hydrogen energy involves mainly 3 steps, the generation, the storage and the energy transfer of hydrogen. In the past two decades, hydrogen storage has become the bottle neck toward the upcoming "hydrogen economy". It is essential for a hydrogen storage media to have high storage capacity, fast sorption kinetics and favorable thermodynamics [3] so that the requirements for commercial hydrogen storage can be satisfied. Since gaseous and liquid state hydrogen storage methods suffer from some serious concerns, such as poor safety and low storage capacity [4], solid state hydrogen storage materials have attracted growing attention in recent years. Among these materials, light metal borohydrides have been extensively investigated as hydrogen carriers owing to their high gravimetric/volumetric hydrogen storage capacity [5]. As one of the light metal borohydrides, Lithium borohydride ($LiBH_4$) receives great attention due to its high gravimetric and volumetric hydrogen density of 18.5 wt. % and 121 kg H_2 m^{-3}, respectively[6-15].

According to the literature, the major decomposition reaction for $LiBH_4$ is [16]: $LiBH_4 \rightarrow LiH+B+3/2H_2$, through which 13.8wt% of hydrogen can be released. However, on account of the high decomposition temperature (above 600^oC) of LiH[17], it is hard for $LiBH_4$ to have a complete dehydrogenation. Furthermore, it is impossible for pure $LiBH_4$to have reversible hydrogen sorption unless a harsh condition (35MPa H_2 and 600^oC) is satisfied for absorption [18]. Hence, extensive researches were done in order to find out a strategy to overcome these obstacles and improve the de/re-hydrogenation properties. One way is to add metal hydrides or metal halides to

form $LiBH_4$ based composite materials [10-22]. For instance, $LiBH_4$-MgH_2[10-13,19-20], $LiBH_4$-$CeCl_3$[21], $LiBH_4$-CeH_2 [22], $LiBH_4$-LiI[14] and other $LiBH_4$-based systems[23-25], as reversible hydrogen storage composites, have already been obtained. These composites showed improved thermodynamic properties and greatly lowered decomposition temperatures compared to $LiBH_4$. To further improve the hydrogen sorption properties of these composites, different catalysts were considered. For example, Wang et al. [26] reported that Ce-based catalysts had distinctive effect on hydrogen storage properties of the $2LiBH_4/MgH_2$ composite. However, some byproducts like B_2H_6appeared as well, resulting in drastically degraded reversible hydrogen capacity [5]. Another way to improve the hydrogen sorption properties of $LiBH_4$ is to confine $LiBH_4$ nanoparticles in porous materials. Gross et al. [27] reported that nanoporous carbon scaffolds would enhance de/re-hydrogenation properties of $LiBH_4$ through "nanoconfinement" effect. Subsequently, mesoporous carbon [28], carbon aerogel nanoscaffolds[29], carbon nanotubes[30], and PMMA-co-BM polymer matrix[31], have been discovered to improve hydrogen sorption thermodynamics and kinetics of $LiBH_4$. Nevertheless, the loading of $LiBH_4$ in these porous materials is fairly low, typically less than 30wt% [27,32], resulting in the low hydrogen sorption capacity. In our recent work, "graphene wrapper" was found to significantly increase the loading of $NaBH_4$ on graphene sheets to 75wt% through nano-encapsulation [33]. The $NaBH_4$@Graphene composite showed stable reversible hydrogen storage of more than 7wt% within 6 cycles. It is also established that the addition of rare earth fluoride (LnF_3) into $NaBH_4$ can form reversible hydrogen storage composites, which show better de/re-hydrogenation properties.

Considering the above, we investigated in this paper, the hydrogen sorption behaviors of two graphene supported $LiBH_4$ composites, namely, $3LiBH_4$/Graphene and $3LiBH_4$/Graphene-10wt%CeF_3 composites. The mechanisms of graphene and CeF_3 on the hydrogen

sorption in $LiBH_4$ are proposed based on experimental results.

2.Experimental

2.1 Sample preparation

Commercially available $LiBH_4$ (purity~95wt.%) was acquired from Aladdin Reagent Database and CeF_3(99.9wt%) was purchased from Alfa Aesar. Graphene containing 5~7wt% of oxygen was obtained from Strem Chemicals Inc., Nanjing XFNANO Materials Tech Co., Ltd., PR China. Handling and operations of these chemicals were carried out under inert atmosphere in an argon-filled glove box (Lab 2000, Etelux Intertgas System Co., Ltd) with a recirculation system to keep H_2O and O_2<1 ppm.

$3LiBH_4$/Graphene composite was prepared through a ball milling method: 0.25g $LiBH_4$ and 0.045g graphene were ball milled for 5 h (Planetary QM-1SP2) under an argon atmosphere at room temperature. The mixture was placed in a 50ml ball-milling vessel together with 11 mm diameter stainless steel balls (the ball-to-powder ratio was 30:1) at 400 rpm. The ball-milling procedure was carried out by alternating 30 min of milling and 30 min of dwelling to avoid drastic temperature rising. The same preparation process was also applied on the $3LiBH_4$/Graphene-10wt%CeF_3 composite, which contains 0.25g $LiBH_4$, 0.045g graphene and 0.033g CeF_3.

2.2 Characterization

The dehydrogenation and rehydrogenation properties were investigated by using a Sievert-type apparatus manufactured by Shanghai Institute of Microsystem and Information Technology. Temperature-programmed-desorption (TPD) measurements were carried out in the temperature range of 25^{o}C to 440^{o}C within 8 h at a heating rate of 3^{o}C min^{-1}. The isothermal dehydrogenation was measured at 425^{o}C starting from vacuum for 6h. The isothermal rehydrogenation was performed at

440^{o}C with an initial 3.3 MPa hydrogen pressure for 11 h.

Differential scanning calorimetry (DSC) analysis of the pure $LiBH_4$and two composites was conducted using synchronous thermal analyzer(Netzsch, STA 449 F3 Jupiter). Samples were heated at a rate of 10 K min^{-1} under 1 bar flowing argon atmosphere with the temperature rising from 25 to 500^{o}C. Up to 4.5mg of sample powder was taken out from the glove box and placed in an alumina crucible for DSC measurements.

The phase component of the composites was characterized by X-ray diffraction(XRD Rigaku D/MAX-2500, VL/PCX, Cu K_{α} radiation). Diffraction patterns were collected at a scanning rate of 5^{o} min^{-1} with a step of 0.02^{o}. To avoid sever oxidation during the XRD measurements, samples were flattened into a homemade container in the glove box.The morphology observations and composition analyses of the composites were conducted using a field emission gun scanning electron microscope (SEM, Hitachi S-4800). Chemical bonding analyses were examined by Fourier transform infrared spectroscope (FT-IR, Nicolet iS5, Thermo Fisher Scientific Inc. U.S.A.) equipped with a horizontal ATR accessory (Germanium crystal) in an argon-filled glove box. Data collection and analyses were carried out by using OMNIC 32 software.

3. Results and discussions

3.1 Characterization of de/re-hydrogenation behaviors

Fig.1 gives the DSC curves of pure $LiBH_4$, 3$LiBH_4$/Graphene and 3$LiBH_4$/Graphene-10wt%CeF_3 composites measured at a heating rate of 10 ^{o}C /min. For comparison, pure $LiBH_4$ was also ball milled using same parameters as the two composites. Clearly, all the curves have three similar endothermic peaks, indicating that the addition of graphene and CeF_3 does not change the main decomposition reaction of $LiBH_4$. Previous investigations showed that heating of pure $LiBH_4$ usually

underwent multiple stages[15-16]. The first peak located about 113°C, the second peak located around 280°C and the third peak started from about 450°C correspond to the structural transition, melting, and decomposition of $LiBH_4$, respectively[34-35]. For the $3LiBH_4$/Graphene and $3LiBH_4$/Graphene-10wt%CeF_3 composites, the three endothermic peaks locate at temperatures close to those for the pure $LiBH_4$.

Fig. 2(a) shows the TPD profiles of ball milled pure $LiBH_4$, $3LiBH_4$/Graphene and $3LiBH_4$/Graphene-10wt%CeF_3 composites with the temperature rising from 20°C to 440°C. As can be seen, the ball milled $LiBH_4$ can release hydrogen at temperature below 100°C, but the amount is lower than that of $3LiBH_4$/Graphene or $3LiBH_4$/Graphene-10wt% CeF_3 composites at the same temperature. The $3LiBH_4$/Graphene released 7.01 wt% of hydrogen when temperature reaches 440°C, while 6.44wt% of hydrogen can be released from the $3LiBH_4$/Graphene-10wt% CeF_3 composite. In comparison, ball milled pure $LiBH_4$ only releases 2.77wt% of hydrogen at 440°C. It was established that pure H_2 can be released in $LiBH_4$-carbon systems [32,36]. Other works[21,37] showed that $LiBH_4$-La(Ce)F_3 and $LiBH_4$-TiF_3 systems did not release F- containing gases and only trace amount of B_2H_6 was released. In addition, our previous work[33] on $NaBH_4$-Graphene systems confirmed that pure H_2 was released during dehydrogenation. Besides, three desorption stages observed in Fig. 2(a) correspond to a small amount of hydrogen release during structural transition, melting and a large amount of hydrogen release during decomposition[16]. The TPD profiles at temperatures lower than 100°C were shown in the inset of Fig. 2(a). It was seen that the $3LiBH_4$/Graphene composite released more hydrogen than the $3LiBH_4$/Graphene-10wt%CeF_3 composite before 86°C, indicating that CeF_3would not catalyze the reaction at low temperatures, while it decreased the contacting area between $LiBH_4$ and graphene, thus lowering down the hydrogen release at low temperatures.

The isothermal dehydrogenation curves of $3LiBH_4$/Graphene and $3LiBH_4$/Graphene-10wt%CeF_3 composites at 425°C starting from vacuum for 6h were presented in Fig. 2(b). Apparently, the addition of CeF_3 significantly accelerated the hydrogen desorption under this condition. For instance, about 6wt% of hydrogen can be released by the $3LiBH_4$/Graphene-10wt%CeF_3 composite within 1 hour, while the $3LiBH_4$/Graphenecomposite releases only 3.5wt% of hydrogen under the same conditions. However, CeF_3 additionalso reduces the total amount of hydrogen released at 425°C.

Fig.3 demonstrates isothermal rehydrogenation profiles of $3LiBH_4$/Graphene and $3LiBH_4$/Graphene-10wt%CeF_3compositesat 440°C with an initial hydrogen pressure of 3.3MPa for 11 h. Clearly, both composites showed rehydrogenation ability under such conditions. Under the same condition, we found that the dehydrogenated pure $LiBH_4$ had hardly any reversibility under present conditions, which was also confirmed in the work of Xu Juan[38] et al. Orimo[18] et al. showed that the dehydrogenated $LiBH_4$ could only be partially rehydrogenated at 600°C under 35MPa hydrogen pressure. We observed that the $3LiBH_4$/Graphene composite absorbed 7.40 wt% of hydrogen to $LiBH_4$ under 3.3 MPa after 11h. However, the one doped with CeF_3 merely absorbed 6.14 wt% of hydrogen to $LiBH_4$ with similar kinetics, indicating that the addition of CeF_3 did not improve rehydrogenation properties of $LiBH_4$. Therefore, we concluded that graphene played a major role in enhancing the reversibility.

3.2 Mechanisms of de/re-hydrogenation

FTIR analyses was used to find out the changes of $[BH_4]^-$ anion in both composites after ball-milling and rehydrogenation. As shown in Fig. 4(a), pure $LiBH_4$ has the characteristic absorption peaks of B-H stretching around 2300 cm^{-1} and a significant splitting of the bending mode at 1095 and 1237cm^{-1}, which reflects the low symmetry of the $[BH_4]^-$ anion in this crystal [39-40].From Figs.4(b)

and 4(c), ball-milled samples of the $3LiBH_4$/Graphene and $3LiBH_4$/Graphene-10wt%CeF_3 composites revealed the characteristic absorption peaks of B-H stretching band at 2361,2313(2327),2276 cm^{-1} and B-H bending band at 1095 and 1237cm^{-1}, quite close to the pure $LiBH_4$ (2361,2307,2276, 1095 and 1237cm^{-1}). The slight shift might be attributed to the charge-transfer from $LiBH_4$ to graphene and CeF_3[33,41], or caused by the FTIR technique itself. Fig.4(d) and 4(e) show the FTIR profiles of the two composite samples at their dehydrogenated state. Clearly, the characteristic absorption peaks of B-H stretching band and B-H bending band disappeared, indicating the completion of dehydrogenation. Instead, we observed an absorption peak assignable to $Li_2B_{12}H_{12}$[42-43] at about 2480 cm^{-1}. In comparison, FTIR profiles of the two rehydrogenated samples were shown in Figs. 4(f) and 4(g). From Fig.4(f), the major peak of B-H stretching band shifted from 2307 cm^{-1} to 2313 cm^{-1}in the rehydrogenated $3LiBH_4$/Graphene composite. As shown in our previous work on $NaBH_4$@Graphene system [33], graphene induced the migration of electron cloud in$[BH_4]^-$, resulting in the weakening of B-H bond. Fig.4(g) showed a more obvious deviation from 2307 cm^{-1} to 2327 cm^{-1}, corresponding to the combined effect of charge transfer to graphene and possible substitution of F^- for H^-[44] in $[BH_4]^-$. In the inset of Fig. 4, the slight shift of absorption peaks after different treatments can be clearly observed. Besides, we observed a weak absorption peak assignable to B-F stretching mode[39] at about 1010 cm^{-1}, which confirmed the possible substitution of F^- for H^-. According to the literature [44], the substitution of F^- for H^- can lead to a favorable modification of hydrogen sorption thermodynamics of borohydrides.

Fig.5 shows the XRD patterns of the $3LiBH_4$/Graphene and $3LiBH_4$/Graphene-10wt%CeF_3 composites under different conditions. As shown in Fig. 5(a), all diffraction peaks were indexed to $LiBH_4$ and no other phases were detected after ball milling. Though the sample contained 25 mol%

of graphene, there was no diffraction peaks from graphene, indicating that graphene was in its amorphous form. Obviously, from Fig. 5(c), the diffraction peaks of $LiBH_4$disappeared after dehydrogenation together with the presence of LiH, indicating the decomposition of $LiBH_4$. Besides, some weak peaks can be assigned to Li_3BO_3 in Fig. 5(c), which is mainly attributed to the reaction between $LiBH_4$ and the oxygen existing in graphene. In Fig.4(d) and (e), the absorption peak assignable to $Li_2B_{12}H_{12}$ can be detected while the XRD results give no trace of it, indicating that only small amount of $Li_2B_{12}H_{12}$ formed during dehydrogenation. We observed that the diffraction peaks of $LiBH_4$ reemerged after rehydrogenation, as shown in Fig. 5(e), showing the regeneration of $LiBH_4$, although the reverse reaction proceeded incompletely, with part of LiH remained. In the meantime, it was also found that Li_3BO_3 was still present and did not participate in the rehydrogenation process. Furthermore, the diminished peak intensity of the regenerated $LiBH_4$suggested a reduction in crystallinity or the creation of amorphous in the rehydrogenated $LiBH_4$ relative to the as-prepared samples [27]. According to the research work of Friedrichs et al. [45], two new species, $Li_2B_{12}H_{12}$ and $Li_2B_{10}H_{10}$, formed during the decomposition of $LiBH_4$, which remained stable even at high temperatures. They also found that $LiBH_4$ was significantly consumed during the formation of $Li_2B_{12}H_{12}$ and $Li_2B_{10}H_{10}$, resulting in much reduced hydrogen release and reversibility[5,46]. In comparison, $Li_2B_{12}H_{12}$ was also detected in the dehydrogenated $3LiBH_4$/Graphene and the $3LiBH_4$/Graphene-10wt%CeF_3 composites by FTIR analyses. However, the $L_{i2}B_{12}H_{12}$ was not detected after rehydrogenation. Thus, the rehydrogenation properties have been improved upon doping with graphene. According to XRD and FTIR results, the hydrogen sorption reaction pathway in the $3LiBH_4$/Graphene composite can be deduced as: $LiBH_4 \overset{Graphene}{\leftrightarrow} LiH + B + 3/2H_2$. XRD patterns showed no trace of boron, indicating that boron existed in an amorphous state.

The same set of XRD patterns of $3LiBH_4$/Graphene-10wt%CeF_3composite were presented in Fig.5. Apparently, the similar process happened except the existence of a new intermediate product due to the addition of CeF_3. From Fig. 5(b), we observed that no reaction occurred after ball milling, while the intensified peaks appeared after dehydrogenation as shown in Fig. 5(d) referred to CeB_6, which was also confirmed by other researchers[22,47]. It demonstrated the stabilization of the dehydrogenated state by the formation of boron compounds instead of pure B [46]. Additionally, a similar phenomenon[41] occurred in the $3NaBH_4$-LnF_3 system makes us believe that CeB_6 is the key issue for the dehydrogenation process, resulting in the increased decomposition kinetics. However, the addition of CeF_3 reduced the absorption capacity, as shown in Fig.3. In comparison, the one only doped with graphene had better performance in reversibility. It suggested that CeB_6kept stable and had no positive effect on rehydrogenation, which was different from what was observed in the $3NaBH_4/CeF_3$ composite [41]. According to the work of Gennari et al. [48], we concluded that the side reaction occurred in the $3LiBH_4$/Graphene-10wt%CeF_3composite can be described as: $6LiBH_4 + CeF_3 \xrightarrow{Graphene} 3LiH + 3LiF + 2CeB_6 + 21/2H_2$. This reaction was irreversible under the present conditions, resulting in the reduced hydrogenation capacity ofthe $3LiBH_4$/Graphene-10wt%CeF_3 composite. Besides, Gosalawit-Utke et al. [49] reported a phenomenon observed in the LiF-MgB_2 system. That was, a $LiBH_{4-x}F_x$ compound formed due to the substitution of F^- for H^-, which played a crucial role in de/re-hydrogenation process. Such a substitution also leads to the formation $LiF_{1-x}H_x$ as LiH and LiF share the same crystal structure and similar lattice parameters[47]. Hence, we cannot distinguish LiF from LiH only on the basis of XRD results.

SEM images given in Fig.6 showed appreciable differences between $3LiBH_4$/Graphene and $3LiBH_4$/Graphene-10wt%CeF_3 composites under different conditions. In Fig. 6(a), the

$3LiBH_4$/Graphene composite agglomerated after ball milling and with some holes and cracks on the surface. For the $3LiBH_4$/Graphene-10wt% CeF_3 composite, the agglomeration during ball milling was more evident, as shown in Fig. 6(b). After rehydrogenation, the morphology of the two composites changed somehow greatly. From Fig. 6(c), we observed that "Macro capsules" formed in the rehydrogenated $3LiBH_4$/Graphene composite with their size over 2mm. These capsules were porous and had lamellar structure on the surface, as shown in Fig.6(d). In comparison, the similar "Macro capsules" were also found in the regenerated $3LiBH_4$/Graphene-10wt%CeF_3 composite, as shown in Figs. 6(e) and 6(f). The differences lied in the fact that the agglomeration was more evident in the $3LiBH_4$/Graphene-10wt%CeF_3 composite: Smaller particles with fewer holes were present with the addition of CeF_3. In the previous work, we observed a homogeneous dispersion of $NaBH_4$[33] on the surface of graphene sheets, preventing the agglomerations. It is believed that the even dispersion and decreasing particle size can benefit both dehydrogenation and rehydrogenation properties of borohydrides [38]. Furthermore, the morphology of rehydrogenated samples shown in Fig.6(d) and (f)refers to the graphene sheets as reported in works by Lian [50] and Wang GX[51] et al. We suggested that $LiBH_4$ was encapsulated in those graphene capsules and reacted on the graphene surface. Tim Mason[52] revealed a wetting mechanism of $LiBH_4$for which partial decomposition of molten $LiBH_4$ produces Li-B defect centers, providing lower$LiBH_4$ cluster/surface energies to get wetting of the pores. Therefore, we concluded that graphene served as the effective heterogeneous nucleation site for $LiBH_4$ during de/re-hydrogenation and enhanced ionic mobility of even dispersion to improve the sorption properties. Consequently, the rehydrogenation mechanism was similar in the $3LiBH_4$/Graphene-10wt%CeF_3 composite except the agglomeration caused by CeF_3 with the decreased reversible capacity.

Based on the above analyses, we conclude that $LiBH_4$ particles can be confined in the graphene sheets after ball milling and due to the loose microstructure of graphene, $LiBH_4$ has a homogeneous dispersion. The special electron configuration of the graphene may induce the destabilization of $LiBH_4$ and the graphene sheets can also confine the decomposition products, such as LiH and B. During rehydrogenation, LiH and B confined in those graphene capsules can be rehydrogenated to form $LiBH_4$. In the $3LiBH_4$/Graphene-10wt%CeF_3 composite, CeB_6 cannot be rehydrogenated, thus the hydrogen absorption capacity is lowered down. However, the formation of CeB_6 plays a key role in dehydrogenation [41], resulting in the improvement of dehydrogenation kinetics.

4.Conclusion

In the present work, the hydrogen sorption behaviors of the $3LiBH_4$/Graphene and $3LiBH_4$/Graphene-10wt%CeF_3 composites prepared through ball milling were investigated. The main results are summarized as follows:

(1) Both the $3LiBH_4$/Graphene and the $3LiBH_4$/Graphene-10wt%CeF_3 composites showed partial hydrogen sorption reversibility. A rehydrogenation capacity of 7.40wt% to $LiBH_4$ could be obtained for the $3LiBH_4$/Graphene at 440°C under 3.3 MPa hydrogen pressure after 11 h. In contrast, the $3LiBH_4$/Graphene-10wt%CeF_3 composite showed faster isothermal desorption kinetics at 425°C but less absorption capacity (6.14wt% to $LiBH_4$) at 440°C.

(2) According to the FTIR and XRD results, the mechanisms of hydrogen sorption in $3LiBH_4$/Graphene and $3LiBH_4$/Graphene-10wt%CeF_3 composites can be proposed as follows. In the $3LiBH_4$/Graphene system, the reaction pathway is: $LiBH_4 \overset{Graphene}{\leftrightarrow} LiH + B + 3/2H_2$. While in the $3LiBH_4$/Graphene-10wt%CeF_3 system, a side reaction involving CeF_3occurred during dehydrogenation and can be deduced as: $6LiBH_4 + CeF_3 \overset{Graphene}{\rightarrow} 3LiH + 3LiF + 2CeB_6 + 21/2H_2$.

Such a reaction was irreversible under present rehydrogenation conditions, resulting in the decreased absorption capacity in the $3LiBH_4$/Graphene-10wt%CeF_3 composite as compared to the one without CeF_3 addition. On the other hand, the newly formed CeB_6 can improve the dehydrogenation kinetics of $3LiBH_4$/Graphene composite.

(3) SEM observations revealed the formation of "graphene capsules" in the $3LiBH_4$/Graphene and $3LiBH_4$/Graphene-10wt%CeF_3 composites after rehydrogenation. Therefore, we conclude that $LiBH_4$ is confined in "graphene capsules", which serve as heterogeneous nucleation sites for $LiBH_4$ during de/re-hydrogenation. Furthermore, the special electronic properties of graphene induce the destabilization of $LiBH_4$ and the confinement of dehydriding products by graphene may improve the reversibility as well.

Corresponding author
* Address correspondence to zoujx@sjtu.edu.cn.

Acknowledgement
Prof. Zou would like to thank the support from the Science and Technology Committee of Shanghai under No. 14JC1491600 and 'Pujiang' project (No. 11PJ1406000). This work is partly supported by Research Fund for the Doctoral Program of Higher Education of China (No. 20100073120007) and from the Shanghai Education Commission (No. 12ZZ017).

References

[1]L. Schlapbach and A. Züttel, Nature, 2001, 414, 353-358.
[2]C. Liu, F. Li, L. P. Ma and H. M. Cheng, Adv. Mater., 2010, 22, E28-E62.
[3]J. Yang, A. Sudik, C. Wolverton and D. J. Siegel, Chem Soc Rev, 2010, 39, 656-675.
[4]R.A. Varin, T. Czujko and Z.S. Wronski, New York, NY: Springer Science&Business Media, 2009.
[5]H. W. Li, Y. G. Yan, S. Orimo, A. Züttel and C.M. Jensen, Energies, 2011, 4, 185-214.
[6]A. Züttel, S. Rentsch, P. Fischer, P. Wenger, P. Sudan, Ph. Mauron and Ch. Emmenegger, J. Alloys Compd., 2003, 356-357, 515-520.
[7]I. Saldan, Cent. Eur. J. Chem.,2011, 9, 761-775.
[8]C. Li, P. Peng, D.W. Zhou and L. Wan, Int. J. Hydrogen Energy, 2011, 36, 14512-14526.
[9]P. Mauron, F. Buchter, O. Friedrichs, A. Remhof, M. Bielmann, C.N. Zwicky and A. Züttel, J. Phys. Chem. B., 2008, 112, 906-910.
[10]U. Bosenberg, S. Doppiu, L. Mosegaard, G. Barkhordarian, N. Eigen, A. Borgschulte, T.R. Jensen, Y. Cerenius, O. Gutfleisch, T. Klassen, M. Dornheim and R. Bormann, Acta Mater., 2007, 55, 3951-3958.
[11]G. Barkhordarian, T. Klassen, M. Dornheim and R. Bormann, J. Alloys Compd., 2007, 440, L18-L21.
[12]J. J. Vajo and S. L. Skeith, J. Phys. Chem. Lett., 2005, 109, 3719-3722.
[13]L. L. Shaw, X. F. Wan, J. Z. Hu, J. H. Kwak and Z. G. Yang, J. Phys. Chem. C, 2010, 114, 8089-8098.
[14]L. H. Rude, E. Groppo, L. M. Arnbjerg, D. B. Ravnsbaek, R. A. Malmkjaer, Y. Filinchuk, M. Baricco, F. Besenbacher and T. R. Jensen, J. Alloys Compd., 2011, 509, 8299-8305.
[15]Y. G. Yan, A. Remhof, S. J. Hwang, H. W. Li, P. Mauron, S. Orimo and A. Züttel, Phys. Chem. Chem. Phys., 2012, 14, 6514-6519.
[16]A. Züttel, P. Wenger, S. Rentsch, P. Sudan, Ph. Mauron and Ch. Emmenegger, J. Power Sources, 2003, 118, 1-7.
[17]A. Zaluska, L. Zaluski and J.O.Ström-Olsen, J. Alloys Compd., 2000, 307, 157-166.
[18]S. Orimo, Y. Nakamori, G. Kitahara, K. Miwa, N. Ohba, S. Towata and A. Züttel, J. Alloys Compd., 2005, 404-406, 427-430.
[19]H.Y. Shao, M. Felderhoff and C. Weidenthaler, J. Phys. Chem. C, 2015, 119, 2341-2348.
[20]P. Sridechprasat, A. Siangsai, B. Kitiyanan, S. Kulprathipanja and P. Rangsunvigit, Clean Technol. Envir., 2015, 17, 1239-1246.
[21]B. J. Zhang, B. H. Liu and Z. P. Li, J. Alloys Compd., 2011, 509, 751-757.
[22]F. C. Gennari, Int. J. Hydrogen Energy, 2011;36:15231-15238.
[23]J. Puszkiel, F. C. Gennari, P. A. Larochette, H. E. Troiani, F. Karimi, C. Pistidda, R. Gosalawit-Utke, J. Jepsen, T. R. Jensen, C. Gundlach, M. Tolkiehn, J. B. Colbe, T. Klassen and M. Dornheim, J.Power Sources, 2014, 267, 799-811.
[24]Y. Pang, Y. F. Liu, X. Zhang, Y. Li, M. X. Gao and H. G. Pan, RSC Adv., 2015, 5, 12144-12151.
[25]I. Saldan, M. Schulze, C. Pistidda, R. Gosalawit-Utke, O. Zavorotynska, L. H. Rude, J. Skibsted, D. Haase, Y. Cerenius, T. R. Jensen, G. Spoto, M. Baricco, K. Taube and M. Dornheim, J. Phys. Chem. C, 2013, 117, 17360-17366.
[26]X. H. Wang, L. Xu, X. C. Wu and C. P. Chen, Rare Metal Mat. Eng., 2011, 40, 1982-1985.
[27]A. F. Gross, J. J. Vajo, S. L. Van Atta and G. L. Olson, J. Phys. Chem. C, 2008, 112(14),

5651-5657.
[28]S. Cahen, J. B. Eymery, R. Janot and J. M. Tarascon, J. Power Sources, 2009, 189, 902-908.
[29]D. T. Shane, R. L. Corey, C. Mclntosh, L. H. Rayhel, R. C. Bowman, J. J. Vajo, A. F. Gross and M. S. Conradi, J. Phys. Chem. C, 2010, 114(9), 4008-4014.
[30]D. Silambarasan, V. J. Surya, V. Vasu and K. Iyakutti, Int. J. Hydrogen Energy, 2011, 36, 3574-3579.
[31]R. Gosalawit-Utke, S. Meerhom, C. Pistidda, C. Milanese, D. Laipple, T. Saisopa, A. Marini, T. Klassen and M. Dornheim, Int. J. Hydrogen Energy, 2014, 39, 5019-5029.
[32]X. F. Liu, D. Peaslee, C. Z. Jost, T. F. Baumann and E. H. Majzoub, Chem. Mater., 2011, 23, 1331-1336.
[33]L. N. Chong, X. Q. Zeng, W. J. Ding, D. J. Liu and J. X. Zou, Adv. Mater., 2015, In press.
[34]F. Pendolina, P. Mauron, A. Borgschulte and A. Züttel, J. Phys. Chem. C, 2009, 113, 17231-17234.
[35]P. Ngene, P. Adelhelm, A. M. Beale, K. P. de Jong and P. E. de Jongh, J. Phys. Chem. C, 2010, 114, 6163-6168.
[36]S. Thiangviriya, R. Gosalawit-Utke, Int. J. Hydrogen Energy, 2015, 4167-4174.
[37]Y. H. Guo, X. B. Yu, L. Gao, G. L. Xia, Z. P. Guo and H. K. Liu, Energy Environ. Sci., 2010, 3, 465-470.
[38]J. Xu, R. R. Meng, J. Y Cao, X. F. Gu, Z. Q. Qi, W. C. Wang and Z. D. Chen, Int. J. Hydrogen Energy, 2013, 38, 2796-2803.
[39]O. Zavorotynska, M. Corno, A. Damin, G. Spoto, P. Ugliengo and M. Baricco, J. Phys. Chem. C, 2011, 115, 18890-18900.
[40]A. M. Racu, J. Schoenes, Z. Lodziana, A. Borgschulte and A. Züttel, J. Phys. Chem. A, 2008, 112, 9716-9722.
[41]L. N. Chong, J. X. Zou, X. Q. Zeng and W. J. Ding, J. Mater. Chem. A, 2015, 3, 4493-4500.
[42]M. P. Pitt, M. Paskevicious, D. H. Brown, D. A. Sheppard and C. E. Buckley, J. Am. Chem. Soc., 2013, 135, 6930-6941.
[43]Y. F. Liu, Y. Zhang, H. Zhou, Y. Zhang, M. X. Gao and H. G. Pan, Int. J. Hydrogen Energy, 2014, 39, 7868-7875.
[44]L. N. Chong, J. X. Zou, X. Q. Zeng and W. J. Ding, J. Mater. Chem. A, 2013, 1, 3983-3991.
[45]O. Friedrichs, A. Remhof, S. J. Hwang and A. Züttel, Chem. Mater., 2010, 22, 3265-3268.
[46]O. Friedrichs, A. Remhof, F. Buchter, S. Orimo and A. Züttel, Phys. Chem. Phys., 2010, 12, 10919-10922.
[47]B. H. Liu, B. J. Zhang and Y. Jiang, Int. J. Hydrogen Energy, 2011, 36, 5418-5424.
[48]F. C. Gennari, L. F. Albanesi, J. A. Pauszkiel and P. A. Larochette, Int. J. Hydrogen Energy, 2011, 36, 563-570.
[49]R. Gosalawit-Utke, J. M. B. von Colbe, M. Dornheim, T. R. Jensen, Y. Cerenius, C. B. Minella, M. Peschke and R. Bormann, J. Phys. Chem. C, 2010, 114, 10291-10296.
[50]P. C. Lian, X. F. Zhu, S. Z. Liang, Z. Li, W. S. Yang and H. H. Wang, Electrochimica Acta, 2010, 55, 3909-3914.
[51]G. X. Wang, X. P. Shen, J. Yao and J. Park, Carbon, 2009, 47, 2049-2053.
[52]T. Mason and E. H. Majzoub, J. Phys. Chem. C, 2014, 118, 8852-8858.

Figure captions

Fig.1 DSC profiles of pure $LiBH_4$ (a), $3LiBH_4$/Graphene (b) and $3LiBH_4$/Graphene-10wt%CeF_3 (c).

Fig.2 TPD curves (a) of pure $LiBH_4$, $3LiBH_4$/Graphene and $3LiBH_4$/Graphene-10wt%CeF_3 composites and their isothermal dehydrogenation curves (b).

Fig.3 Isothermal rehydrogenation curves of $3LiBH_4$/Graphene and $3LiBH_4$/Graphene-10wt%CeF_3 composite samples measured at 440^oC under 3.3MPa hydrogen pressure.

Fig.4 FTIR spectra of pure $LiBH_4$ (a), $3LiBH_4$/Graphene (b) and $3LiBH_4$/Graphene-10wt%CeF_3 (c) composites after ball-milling, $3LiBH_4$/Graphene (d) and $3LiBH_4$/Graphene-10wt%CeF_3 (e)after dehydrogenation and $3LiBH_4$/Graphene (f) and $3LiBH_4$/Graphene-10wt%CeF_3 (g) after rehydrogenation.

Fig.5 X-ray diffraction patterns of the ball-milled $3LiBH_4$/Graphene (a) and $3LiBH_4$/Graphene-10wt%CeF_3 (b) composite samples, the dehydrogenated $3LiBH_4$/Graphene (c) and $3LiBH_4$/Graphene-10wt%CeF_3 (d) composite samples and the rehydrogenated $3LiBH_4$/Graphene (e) and $3LiBH_4$/Graphene-10wt%CeF_3 (f) composite samples.

Fig.6 Typical SEM images of ball-milled $3LiBH_4$/Graphene(a) and $3LiBH_4$/Graphene-10wt%CeF_3(b), rehydrogenated $3LiBH_4$/Graphene (c: low magnification; d: high magnification) and $3LiBH_4$/Graphene-10wt%CeF_3(e: low magnification; f: high magnification).

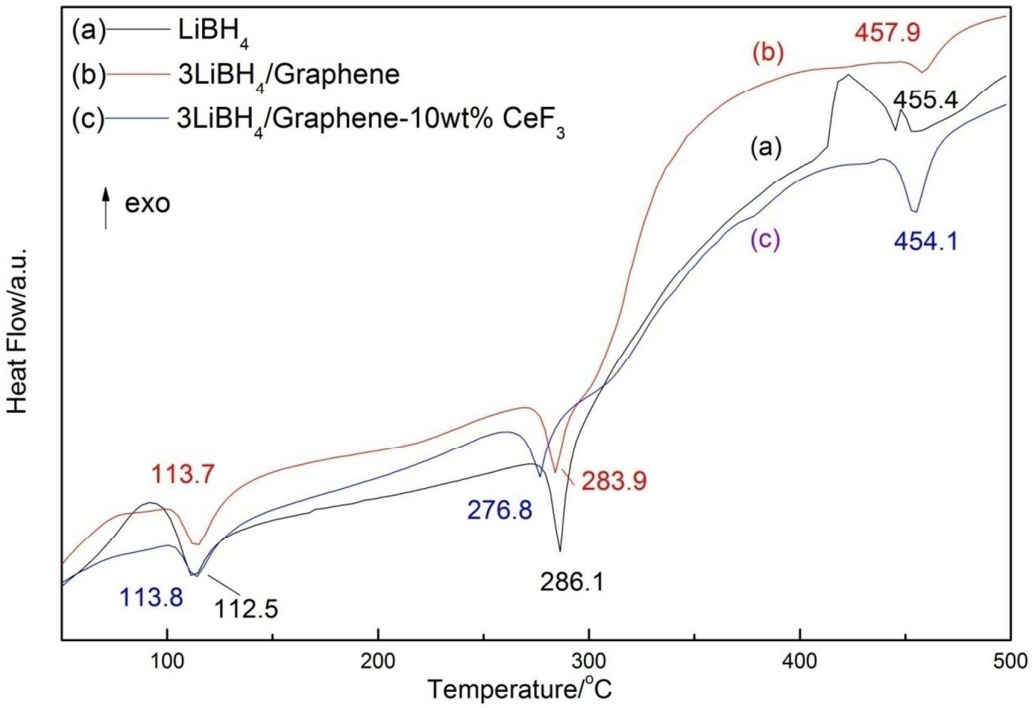

Fig.1 DSC profiles of pure $LiBH_4$ (a), $3LiBH_4$/Graphene (b) and $3LiBH_4$/Graphene-10wt%CeF_3 (c).

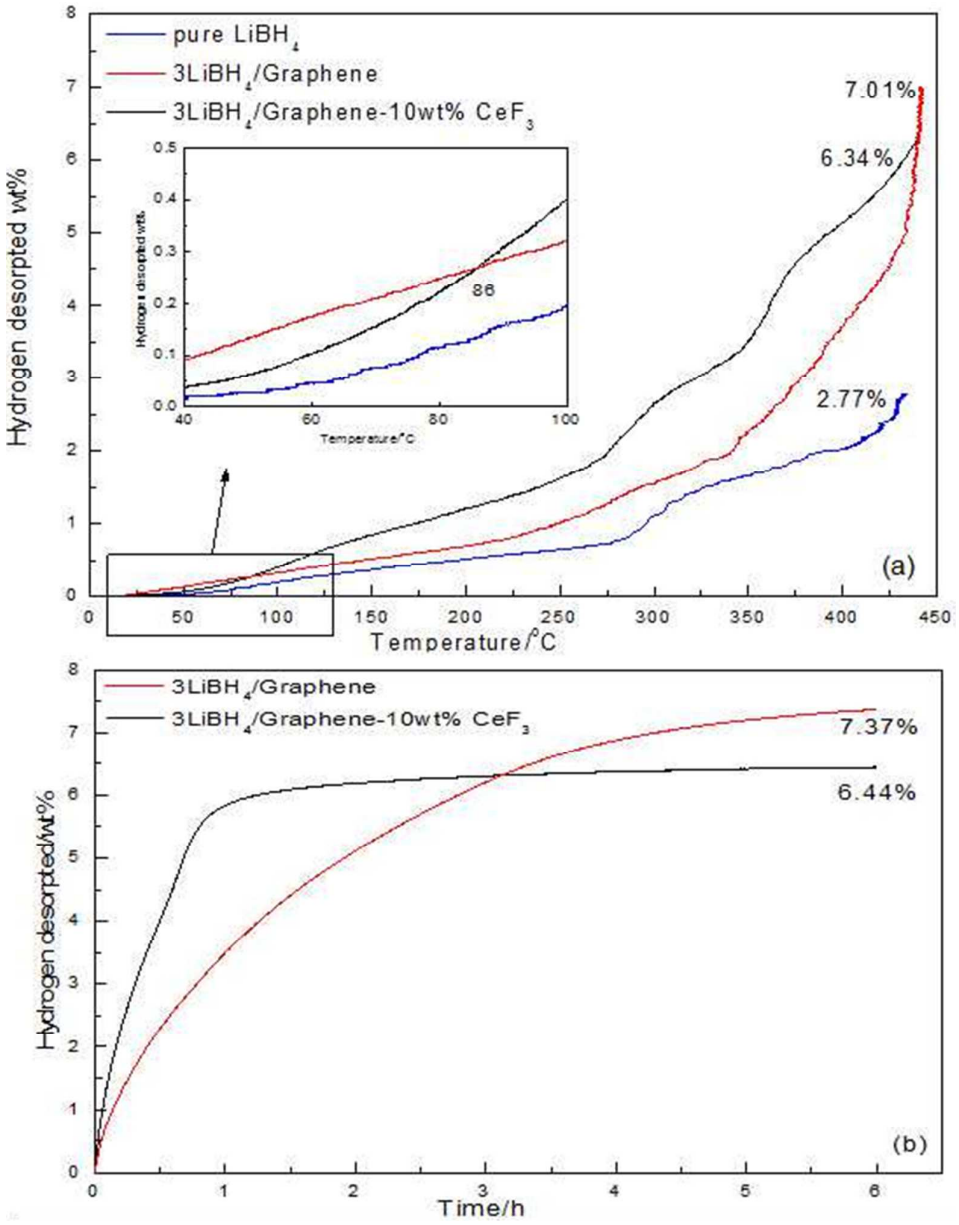

Fig.2 TPD curves (a) of pure $LiBH_4$, $3LiBH_4$/Graphene and $3LiBH_4$/Graphene-10wt%CeF_3 composites and their isothermal dehydrogenation curves (b).

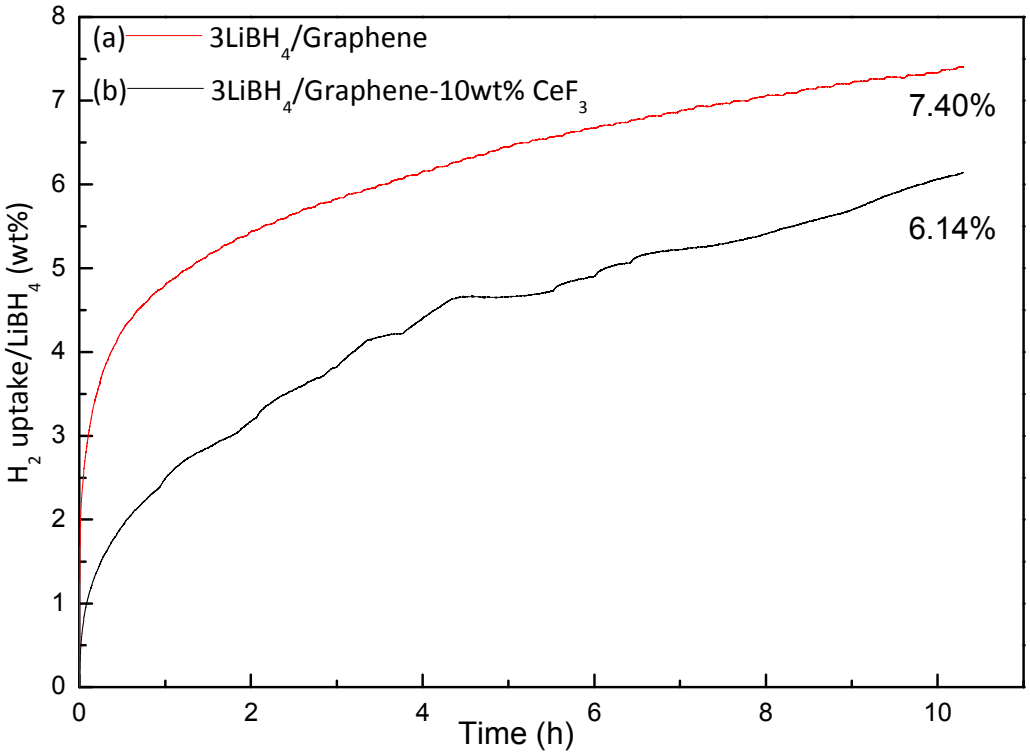

Fig.3 Isothermal rehydrogenation curves of $3LiBH_4$/Graphene and $3LiBH_4$/Graphene-10wt%CeF_3 composite samples measured at 440°C under 3.3MPa hydrogen pressure.

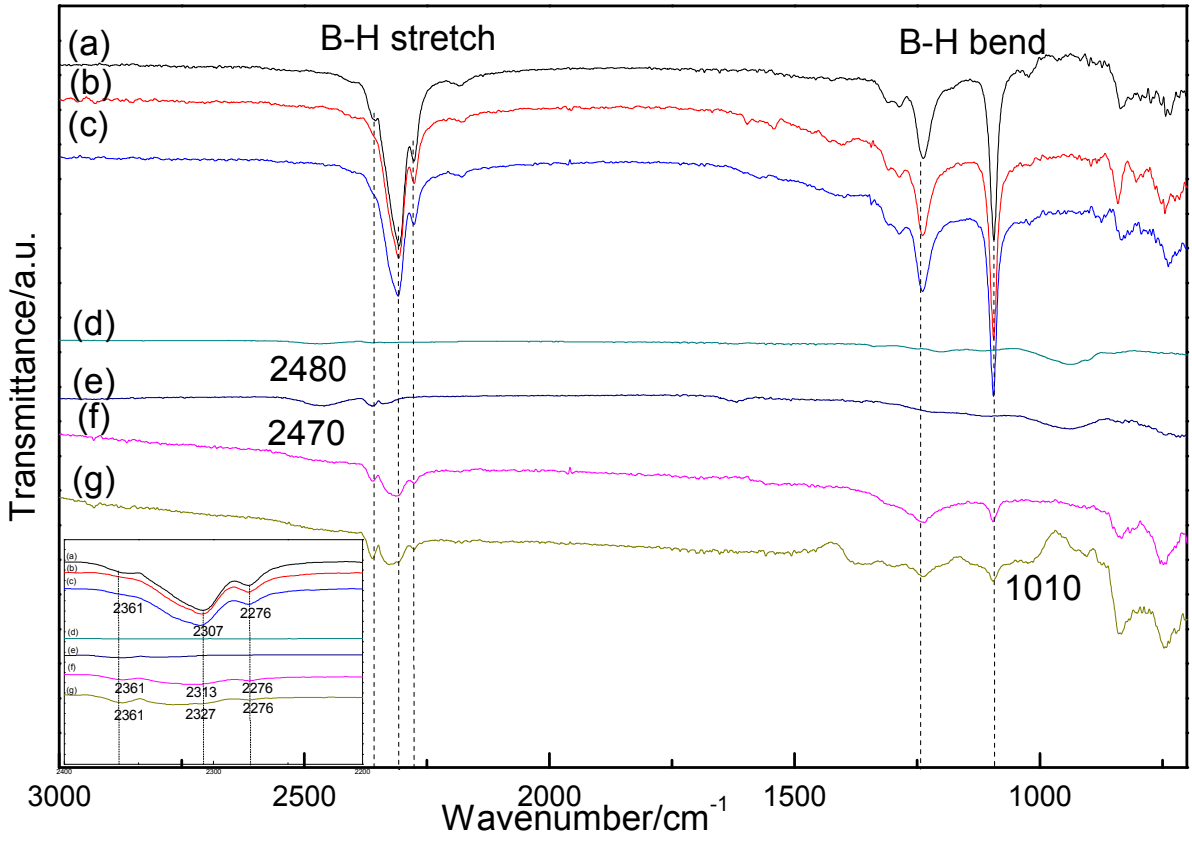

Fig.4 FTIR spectra of pure $LiBH_4$ (a), $3LiBH_4$/Graphene (b) and $3LiBH_4$/Graphene-10wt%CeF_3 (c) composites after ball-milling, $3LiBH_4$/Graphene (d) and $3LiBH_4$/Graphene-10wt%CeF_3 (e) after dehydrogenation and $3LiBH_4$/Graphene (f) and $3LiBH_4$/Graphene-10wt%CeF_3 (g) after rehydrogenation.

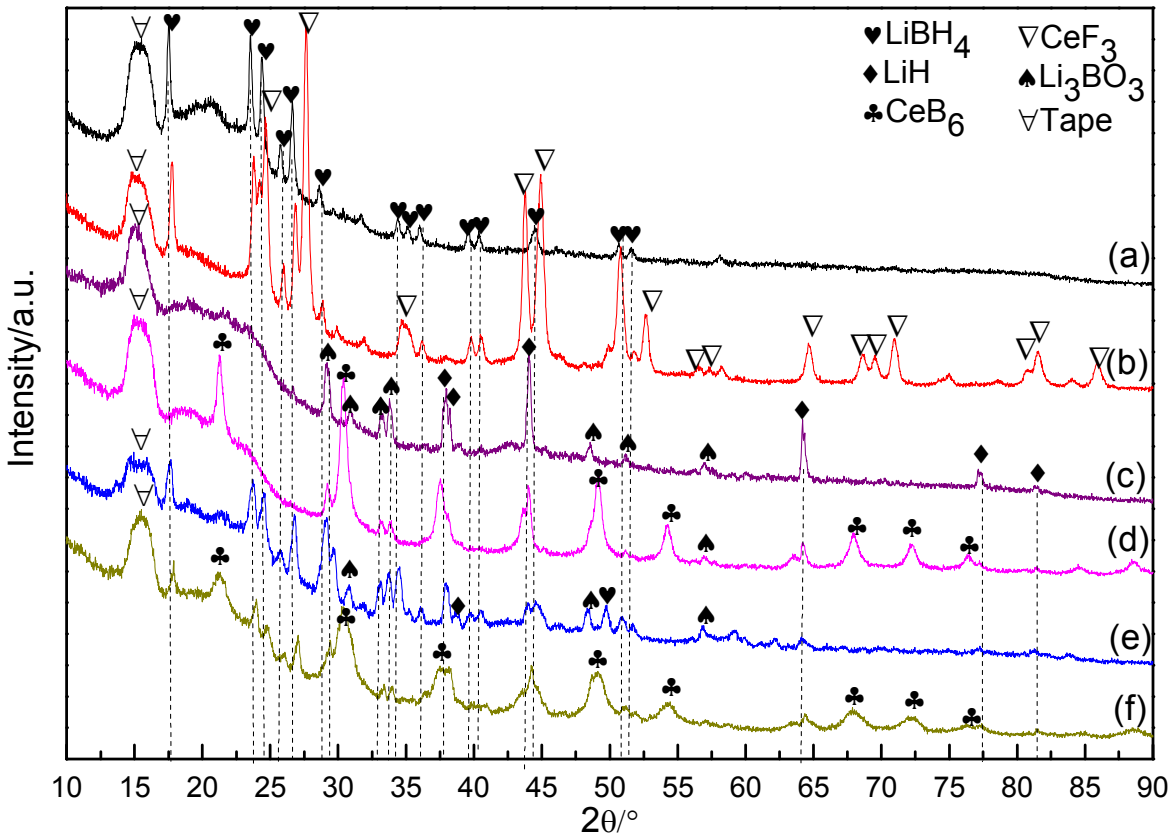

Fig.5 X-ray diffraction patterns of the ball-milled $3LiBH_4$/Graphene (a) and $3LiBH_4$/Graphene-10wt%CeF_3 (b) composite samples, the dehydrogenated $3LiBH_4$/Graphene (c) and $3LiBH_4$/Graphene-10wt%CeF_3 (d) composite samples and the rehydrogenated $3LiBH_4$/Graphene (e) and $3LiBH_4$/Graphene-10wt%CeF_3 (f) composite samples.

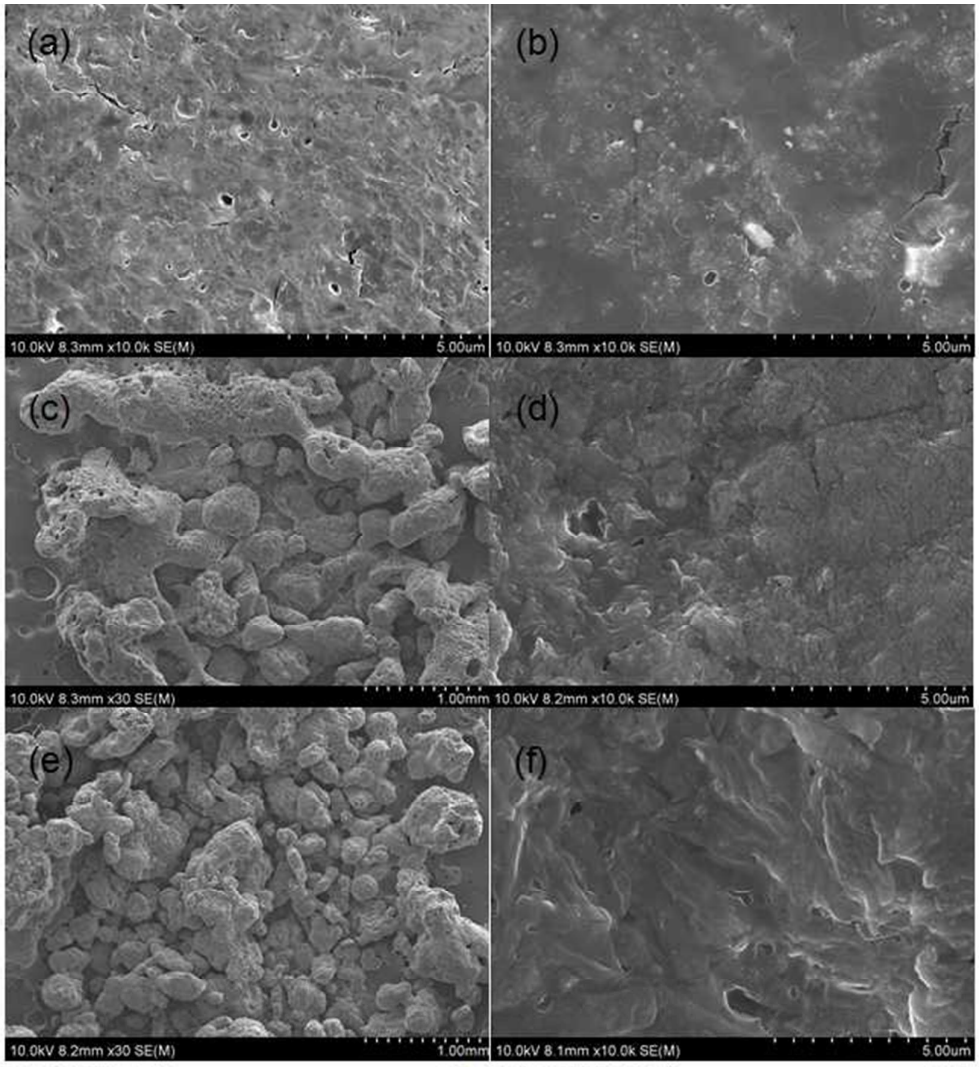

Fig.6 Typical SEM images of ball-milled $3LiBH_4$/Graphene (a) and $3LiBH_4$/Graphene-10wt%CeF_3 (b), rehydrogenated $3LiBH_4$/Graphene (c: low magnification; d: high magnification) and $3LiBH_4$/Graphene-10wt%CeF_3 (e: low magnification; f: high magnification).